Available online at www.sciencedirect.com
SCIENCE DIRECT®
Polymer 44 (2003) 3319–3325
polymer
www.elsevier.com/locate/polymer

Conductivity model and photoacoustic FT-IR surface depth profiling of heterogeneous polymers

Kalpana S. Katti[1], Marek W. Urban*

Department of Polymer Science, School of Polymers and High Performance Materials, The University of Southern Mississippi, Box 10076 Hattiesburg, MS 39406-0076, USA

Received 17 January 2003; accepted 12 February 2003

Abstract

A novel thermal model is developed for surface depth profiling of heterogeneous polymeric surfaces using step-scan photoacoustic Fourier transform (SS PA FT-IR) spectroscopy. This approach is based on the propagation of thermal waves generated during the photoacoustic effect which travel to the film–air (F–A) interface, thus generating acoustic signals above the surface, which upon Fourier transform, result in infrared spectra. The developed model volumetrically slices the surface into finite homogeneous layers parallel to the film–air (F–A) interface and a composition of each *i*th layer is assumed to be the same, but the layers among themselves (*i*th + 1 and *i*th − 1) may or may not exhibit compositional changes. Overall thermal properties of the multi-layered surface consist of the sum of in-series connected thermal conductor layers. The proposed model can be utilized to polymeric films containing the following parametrically analyzed inclusions: (1) inclusions with no interphase between the matrix polymeric and (2) inclusions with a finite interphase. This model is flexible, allowing variations of the particle size, shape, and surface/interfacial microstructural changes. It was tested for depths of penetrations in the range of 5–50 μm for carbon black inclusions imbedded into a two-component (2K) polyurethane (PUR) film deposited on acrylonitrile–butadiene–styrene (ABS) substrate. These studies show that the experimental results are consistent with the proposed model, allowing predictions of interphase layers on particles; for example, a 10 nm water layer adsorbed on carbon black particle surfaces can be detected.

Keywords: Heterogeneous polymers; Carbon black; Photoacoustic phenomena

1. Introduction

Although the first demonstration of photoacoustic phenomena appeared in 1880 [1], experimental and theoretical formulations were formulated in the last two and a half decades [2–11]. Unlike other vibrational spectroscopic techniques, such as attenuated total reflectance (ATR) [4] spectroscopy, which depend on the optical properties of a material, generation of a photoacoustical signal depends both on the optical and thermal properties. This may be considered disadvantageous because it is often difficult to isolate thermal properties of a material and different time domains of optical and thermal responses may lead to rather involved analysis of interactions. In general, non-radiative photoacoustic signal generation process occurs when electromagnetic radiation is adsorbed, and as a result of reabsorption, thermal waves are generated near the surface [5]. The Rosenscwaig and Gersho (R–G) theory [2,11] predicted that for homogeneous materials, thermal diffusion length μ_{th} can be achieved in PAS by changing the modulation frequency, f, which for interferometric detection is accomplished by changing the modulation frequency of the moving mirror. If this is combined with the step-scan (SS) mode of the interferometric detection, a constant depth of penetration for all wavenumbers will be achieved through:

$$\mu_{th} = \sqrt{\frac{K}{\rho C \pi f}} \tag{1}$$

where K, r, and C are conductivity, density and specific heat content, the intrinsic thermal properties of the material. Although this useful relationship allows estimations of distances from which signal is obtained, its inherent drawbacks are the frequency dependence and thermal

* Corresponding author. Tel.: +1-601-266-6454; fax: +1-601-266-5635.
E-mail address: marek.urban@usm.edu (M.W. Urban).
[1] Permanent address: Civil Engineering, North Dakota State University, Fargo, ND 58105, USA.

0032-3861/03/$ - see front matter © 2003 Elsevier Science Ltd. All rights reserved.
doi:10.1016/S0032-3861(03)00187-3

property changes for non-homogeneous surfaces. While the frequency dependence can be eliminated by the use of step-scan interferometric detection [12], thermal non-homogeneity of polymeric films and coatings resulting from either stratification processes during film formation [13–15] or crosslinking reactions [16,17] or purposely introduced dispersed phases such as pigments, fillers, and additives [18,19] is a major problem, especially when quantitative analysis is needed. In view of the above considerations it is thus important to be able to estimate penetration depths probed using variable modulation frequencies using step-scan step-scan photoacoustic Fourier transform (SS PA FT-IR) for non-homogeneous systems. This requires an estimation of the thermal and optical properties of 'composite' materials that consist of a polymer matrix and inclusions.

2. Theoretical formulation of the two step polymer composite model

We consider a polymeric coating that is volumetrically sliced into n equal volume virtual components in the direction perpendicular to the coating-interface. Each of the sliced layers represents a unique material with unique thermal properties of conductivity (K_i), specific heat (C_i), and density (ρ_i), thus being homogeneous, whereas layers among themselves are not. Thus, the composite model consists of a two-step process: (1) the entire volume is sliced into finite number (n) of equisized internally homogeneous layers and thermal properties of the composite are calculated by regarding the coating-inclusion system as a series conduction system with all the layers connected in series, and (2) each layer is regarded as a composite of two or more phases with similar thermal properties. The thermal properties of each layer are calculated from the volume fraction average laws, and the $(i+1)$th layer from the properties of each ith layer. The general approach of this two-step process in determining thermal properties of the composite is shown in Fig. 1. In the first step, the total thermal conductivity is represented by the entire volume of a coating, as a series conductor with the total conductivity given by

$$\frac{1}{K} = \sum_{i=1}^{n} \frac{v_i}{K_i} \tag{2}$$

where K_i and ν_i are the conductivity and the volume fraction of each layer. Since the layers are equisized, $\nu_i = 1/n$, and Eq. (2) reduces to:

$$K = \frac{n}{\sum_{i=1}^{n} \frac{1}{K_i}} \tag{3}$$

The density and the specific heat of the composite are given

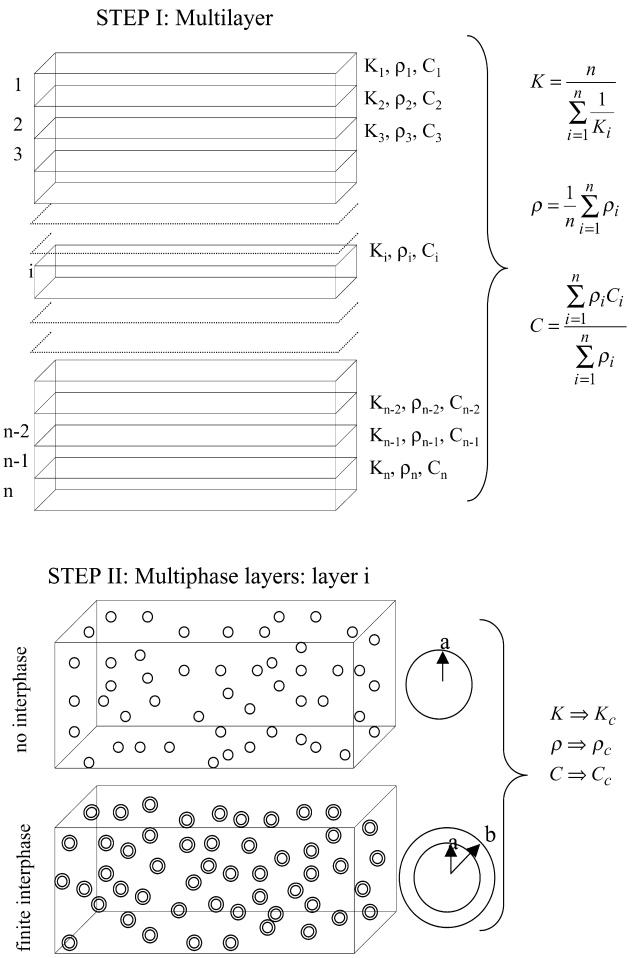

Fig. 1. Schematic diagram of the two-step process for computing thermal properties of polymeric films containing inclusions.

by the volume fraction averages as follows:

$$\rho = \frac{1}{n} \sum_{i=1}^{n} \rho_i \tag{4}$$

$$C = \frac{\sum_{i=1}^{n} \rho_i C_i}{\sum_{i=1}^{n} \rho_i} \tag{5}$$

In order to calculate the thermal properties of each layer, IR bands in SS PA FT-IR spectra for the two different phases 1 and 2 due to stratification processes are identified. Normalized band area ratios are plotted as a function of 'arbitrary' depth of penetration, as determined from the thermal properties of pure components. Statistically, best fit curves are obtained, which is given by $g(x)$. For a two phase system, volume fractions of phases A and B in ith layer is given by $g(i/n)/(\rho' + g(i/n))$ and $\rho'/(\rho' + g(i/n))$, where ρ' is the ratio of densities of the two phases. Thermal conductivity, density, and specific heat for the ith layer can thus be obtained from the volume fractions of the two

phases. This is given by:

$$K_i = \left[\frac{g(i/n)}{\rho' + g(i/n)}\right]K_A + \left[\frac{\rho'}{\rho' + g(i/n)}\right]K_B \quad (6)$$

$$\rho_i = \left[\frac{g(i/n)}{\rho' + g(i/n)}\right]\rho_A + \left[\frac{\rho'}{\rho' + g(i/n)}\right]\rho_B \quad (7)$$

$$C_i = \frac{\rho_A C_A\left[\frac{g(i/n)}{\rho' + g(i/n)}\right] + \rho_B C_B\left[\frac{\rho'}{\rho' + g(i/n)}\right]}{\rho_A\left[\frac{g(i/n)}{\rho' + g(i/n)}\right] + \rho_B\left[\frac{\rho'}{\rho' + g(i/n)}\right]} \quad (8)$$

where K_A and K_B are thermal conductivities, ρ_A, ρ_B are densities and C_A, C_B are specific heats of phases A and B, respectively. Considering addition of inclusions, thermal properties of each layer can be further modified and we will consider two cases: (1) an intimate thermal contact between an inclusion and a polymer matrix, and (2) an interphase between an inclusion and a polymer matrix. The presence of adsorbed phases on the surface of the inclusions and debonding of the inclusions from the coating are two examples where such an interphase may exist.

2.1. Case 1. Interfacial film-inclusion contact

Hasselman et al. [20–24] used an equivalent inclusion concept to estimate the thermal conductivity of a composite consisting of a matrix with inclusions. The essence of this model is to equate thermal disturbances created by m particles to that generated by a single particle of conductivity k_{eff} and volume mV/c, where c is the volume fraction of the inclusions in the matrix. The equivalent inclusion is an ellipsoid with semiaxes α, β, and γ that are related to the individual inclusion axes as, $\alpha/a = \beta/b = \gamma/c$ and $m(abc)/(\alpha\beta\gamma) = c$. An expression for the thermal conductivity of a composite K_{eff} can be derived for general ellipsoidal inclusions [25],

$$K_{eff} = K\left[1 + \frac{(\sigma - 1)c}{(\sigma - 1)(1 - c)h_k + 1}\right] \quad (9)$$

where σ is the conductivity ratio of inclusion and coating and h_k is the inclusion shape factor given by:

$$h_k = \frac{abc}{2}\int_0^\infty \frac{dt}{(a^2 + t)\sqrt{(a^2 + t)(b^2 + t)(c^2 + t)}} \quad (10)$$

which reduces to 1/3 for spherical inclusions.

Combining the proposed layered coating system and modified version of the thermal model [25], the thermal conductivity of the ith layer in the presence of inclusions is represented as:

$$K_{i\_inc} = K_i\left[1 + \frac{(\sigma_i - 1)c}{(\sigma_i - 1)(1 - c)h_k + 1}\right] \quad (11)$$

where K_i is the conductivity of the ith matrix layer determined by Eq. (5). The density and specific heat of the ith layer are calculated from the volume fraction averages as follows:

$$\rho_{i\_inc} = \rho_i(1 - c) + \rho_{inc}c \quad (12)$$

$$C_{i\_inc} = \frac{\rho_i C_i(1 - c) + \rho_{inc}C_{inc}c}{\rho_i(1 - c) + \rho_{inc}c} \quad (13)$$

where ρ_{inc} and C_{inc} are the density and the specific heat of inclusion. Using the series conductor model described earlier, the total thermal parameters can be calculated using Eqs. (3)–(5).

2.2. Case 2. Inter-phase film-inclusion contact or debonding

In the presence of an interphase between an organic coating phase and an inclusion, the thermal parameters, particularly the conductivity of the composite is significantly altered. This is because an interphase acts as a thermal barrier, such as that for high conductivity inclusions debonded from an organic matrix, or for high conductivity inclusions coated on the surface with a low conductive layer y. In the latter case inclusions can enhance conductivity of a composite. It should be noted that significant effects of interfacial characteristics on thermal properties have been demonstrated for particulate- and fiber-reinforced composites [25], but no account beyond the volume fraction was anticipated. Although Bruggeman [26] introduced an effective medium approach which was further modified [27], this model did not take into account the fact that inclusions may exhibit interfacial layers. Empirical models, such as derived by Agari et al. [28–31] are specific for the case of high conductivity inclusions as well as the large volume fractions of inclusions. Finite element modeling [32] of such composites have yielded accurate predictions of thermal properties, but does not provide insights into the nature of the physical phenomena of the heat conduction in such composites.

With this in mind let use the effective medium concept, for which the self-consistency condition given by:

$$(1 - c')\frac{1 - \sigma_c}{1 + 2\sigma_c} + c'\frac{\left(\frac{b}{a}\right)^3\frac{\sigma_3 - \sigma_c}{\sigma_3 + 2\sigma_c} + \beta_{23}\frac{2\sigma_3 + \sigma_c}{\sigma_3 + 2\sigma_c}}{\left(\frac{b}{a}\right)^3 + 2\beta_{23}\frac{\sigma_3 - \sigma_c}{\sigma_3 + 2\sigma_c}} = 0 \quad (14)$$

where c' is the total volume fraction of inclusion and interphase, σ_3 is conductivity ratio of interphase and coating, b and a are the radii of interphase and the inclusion, and σ_c is the conductivity ratio of composite conductivity of coating. For a given thickness of the interphase layer c' is equal to $c(b/a)^3$ for spherical inclusions. Furthermore, β_{ij} is a measure of thermal disparity between i and j materials and

is given by:

$$\beta_{ij} = \frac{k_i - k_j}{k_i + 2k_j} = \frac{\sigma_i - \sigma_j}{\sigma_i + 2\sigma_j} \quad (15)$$

In an effort to estimate thermal parameters of each layer in the coating system, Eq. (14) is solved for each of the n layers with the unpigmented coating conductivity given by Eq. (6). As before, specific heat and density of ith layer is given by:

$$\rho_{i\_inc\_int} = \rho_i(1 - c') + \rho_{inc}c + \rho_{int}(c' - c) \quad (16)$$

$$C_{i\_inc\_int} = \frac{\rho_i C_i(1 - c') + \rho_{inc}C_{inc}c + \rho_{int}C_{int}(c' - c)}{\rho_i(1 - c') + \rho_{inc}c + \rho_{int}(c' - c)} \quad (17)$$

Again, using the series conductor model described earlier, the total thermal parameters can be calculated using Eqs. (3)–(5). The flowchart illustrating the general methodology of thermal property calculations described above is shown in Fig. 2.

3. Experimental spectroscopic data aquisition

Photoacoustic FT-IR spectral measurements were performed using a PA cell (Model 300 MTEC) and a Nicolet 850 Series II FT-IR spectrometer. For step-scan (SS) PAS spectral acquisition, a resolution of 8 cm^{-1} and modulation frequencies ranging from 25 to 1000 Hz were used. All sample spectra were ratioed against carbon black (MTEC Industries) spectra recorded under identical conditions. Data acquisition was obtained using Omnic FT-IR software (Nicolet Instrument Corp.) and spectral calculations were performed using Grams 32 software (Galactic Industries Corp.).

Carbon pigmented 2-component (2K) PUR coatings at 0, 5, and 10% pigment volume levels (PVC) were formulated and cast on ABS substrates using the procedure described elsewhere [33]. Deconvoluted spectra were generated from the best estimation of a maximum probability approach using physical information about spectral features and statistical knowledge of the number of overlapping bands. SSRES software is utilized for this purpose.

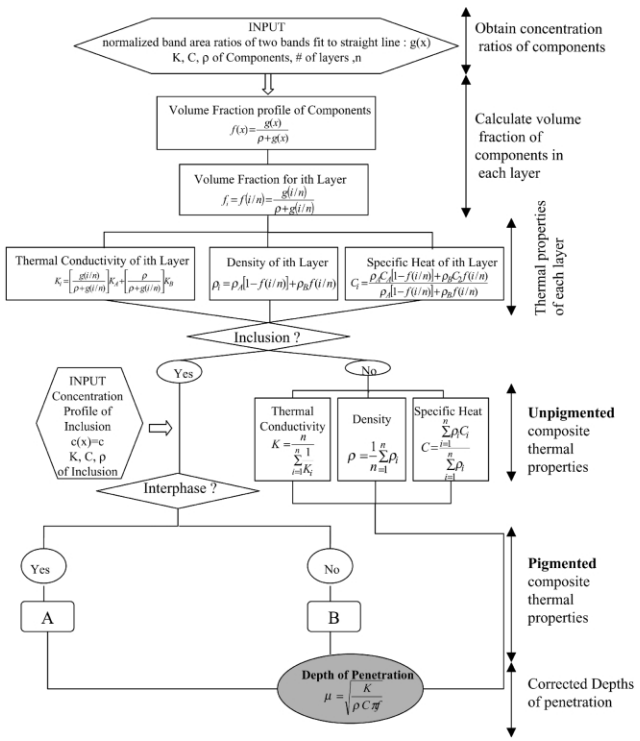

Fig. 2. Flowchart for estimating the depth of penetration from SS PA FT-IR spectra in polymeric films containing inclusions. Algorithms labeled as A and B are included in Appendix A.

4. Results and discussion

SS PA FT-IR spectra were acquired on PUR films using a range of modulation frequencies ranging from 50 to 1000 Hz. The C–H region of the spectra for 0% PVC are shown in Fig. 3, traces B–F. The spectra were normalized to the 2952 cm^{-1} band. For reference purposes, the pure component spectra of PUR and ABS are shown in traces A and G. As seen, the aromatic C–H stretching vibrations due to ABS at 3027 and 3061 cm^{-1} are detectable for the 0% PVC sample. For a 50 Hz modulation frequency (Trace F), the presence of the 3027 and 3061 cm^{-1} bands is being detected and aromatic C–H stretching bands for 0% PVC sample at 200 Hz are present. On the other hand, the same two bands begin to be detected for a 10% PVC at 400 Hz, as seen in Trace C, Fig. 4. These observations indicate for pigmented PUR deeper penetration depths are obtained using the same modulation frequencies.

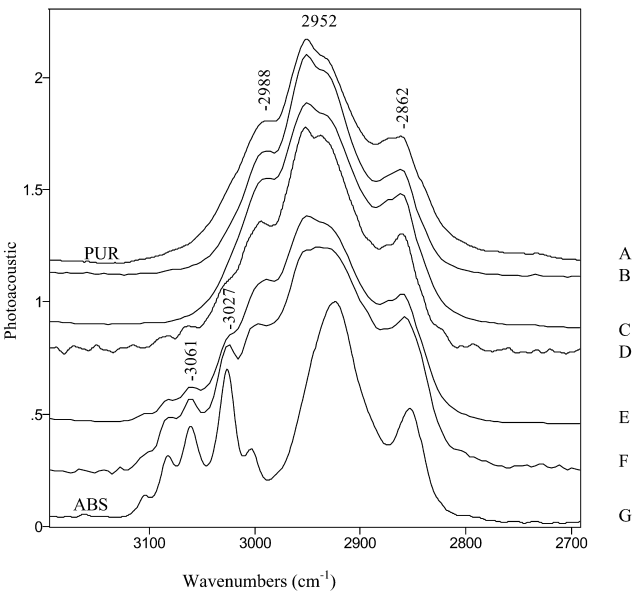

Fig. 3. SS PA FT-IR spectra in the C–H stretching region for 0% PVC PUR coating on ABS acquired at 1000 Hz (B), 400 Hz (C), 200 Hz (D), 100 Hz (E) and 50 Hz (F). Traces A and G are PUR and ABS SS PA FT-IR spectra, respectively.

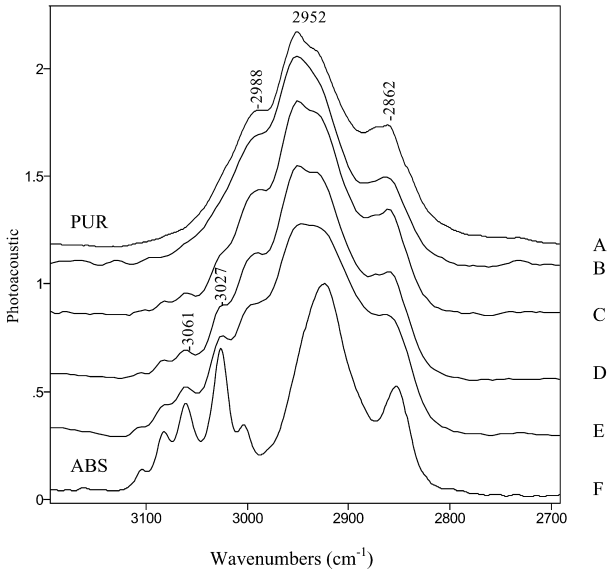

Fig. 4. SS PAS spectra in the C–H stretching region for 10% PVC PUR coating on ABS acquired at 1000 Hz (B), 400 Hz (C), 200 Hz (D), and 50 Hz (E). Traces A and G are PUR and ABS SS PA FT-IR spectra, respectively.

Furthermore, previous studies [19] have shown that polyurea (PUA) coexists with PUR for 2K PUR films, and the extent of PUA formation is influenced by the presence of OH and H_2O functionalities on the surface of carbon black particles. The above data was obtained by plotting the band area ratio of the 1752 and 1733 cm^{-1} bands as a function of the depth of penetration. As shown in Fig. 5, the area ratios are fitted to straight lines for 0% PVC, 5% PVC and 10% PVC samples, and Table 1 lists the best fit line parameters for the 0, 5, and 10% PVC samples.

Using the thermal properties of the individual components which are summarized in Table 2, let us test the proposed model and volumetrically slice the surface into 100 equisized layers. Using the methodology described in Section 3, the thermal parameters of non-pigmented coating were calculated for the PUR/PUA stratification processes.

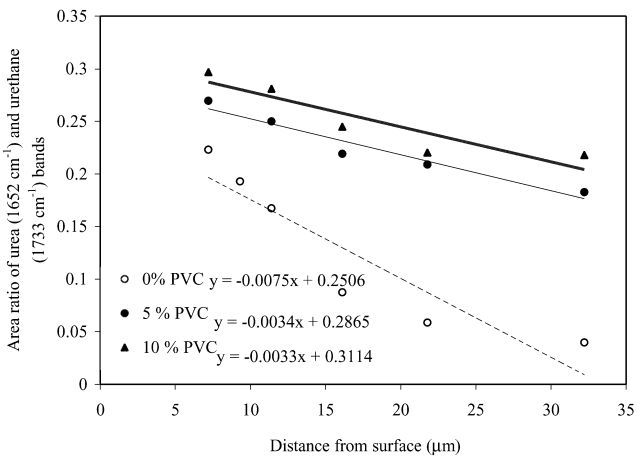

Fig. 5. The band area ratio of the 1652 and 1733 cm^{-1} bands plotted as a function of penetration depth for homogeneous PUR polymer films.

Table 1
Fitting parameters from Fig. 5

PVC (%)	$g(x) = A + Bx$	
	A	B
0	−0.007489	0.250626
5	−0.003413	0.286523
10	−0.003334	0.311428

Fig. 6 shows the effect of stratification of PUA on the penetration depth. As seen, stratification appears to be quite significant.

At this point let us evaluate the effect of carbon black pigmentation on photoacoustic depth penetration. The fitting parameters of 0, 5, and 10% PVC from Table 1 were utilized for the purpose. Thus, the influence of inclusion particles on the composite conductivity is two faceted: (1) by altering the PUA/PUR ratio across coating thickness, and (2) by the influence on thermal conduction processes due to the difference in coating-pigment conductivities. Thus, the composite conductivity is modeled using the approach outlined in Section 3 combined with the layering concept of the coating using the fitting parameters summarized in Table 1. While the effect of inclusions on conductivity are summarized in Fig. 7, it should be kept in mind that this approach assumes a uniform incorporation of pigment particles across the film thickness.

Analysis of the data shown in Fig. 7 clearly indicates that increased PVC also result in the increase of the depth of penetration into the coating for all modulation frequencies. Since adsorbed layer of water exists on the surface of carbon black particles [33], its presence may dramatically influence the composite conductivity and thus the penetration depth from which the signal is detected. For that purpose the self-consistency equation in Eq. (14) was solved for each of the 100 layers for various interphase thicknesses. The results of these calculations are shown in Fig. 8 and indicate that going from 0.5 to 50 nm thick interphase in 10% PVC, the depth from which signal is detected increases. Although the interphase exhibits lower conductivity than the inclusion particles, yet its conductivity is certainly higher than that of an organic phase. Thus, its overall conductivity is enhanced under an effective medium approach. It should be also noted that when the interface is thickness, it eventually acts as a thermal barrier on inclusion particle and reduces the overall

Table 2
Physical properties of individual components

	K, conductivity (W/m/K)	Density (kg/m^3)	Specific heat (J/kg/K)
Polyurethane (PUR) [34]	0.23	1050	1340
Polyurea (PUA) [34]	0.29	1066	1240
Carbon Black [35]	129	174.601	709
Water [35]	0.6069	996.93	4180

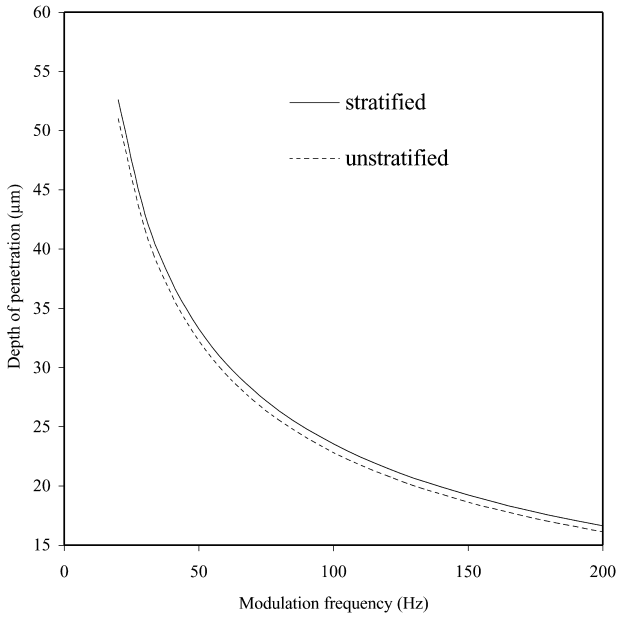

Fig. 6. Depth of penetration plotted as a function of modulation frequency for stratified and non-stratified PUR films.

conductivity. As a result, the depth from which the signal is detected eventually will decrease (Fig. 8). Furthermore, as seen in Figs. 3 and 4, the depth of penetration at 400 Hz modulation frequency for pigmented PUR coatings corresponds to that observed at about 200 Hz for unpigmented coatings. The data presented in Fig. 8 shows that this signal corresponds to the interphase thickness of about 10 nm.

5. Conclusions

The objective of this study was to develop a thermal depth-profiling model for estimating the depth of penetration using SS PA FT-IR for polymeric film containing inclusions. Two specific cases were parametrically analyzed: (1) inclusions bonded in the organic phase and no interphase between the organic phase and inclusion particles was assumed, and (2) the presence of an finite interphase between an organic phase and inclusion. These studies showed that the essence of the proposed model lies in volumetrically slicing coating thickness numerically into finite homogeneous layers perpendicular to the film–air interface. Using a step-wise layer model, the total thermal properties of the film are calculated using a series conductor model and the thermal properties for each layer are calculated using earlier literature thermal models. Although the developed model was tested for PUR containing carbon black particles, this model is general and can be utilized to different particle sizes, shapes, and microstructures, thus it is general. Analysis of the experimental PA FT-IR data indicates that the sensitivity levels of the particle–matrix interphase can be in the nm range.

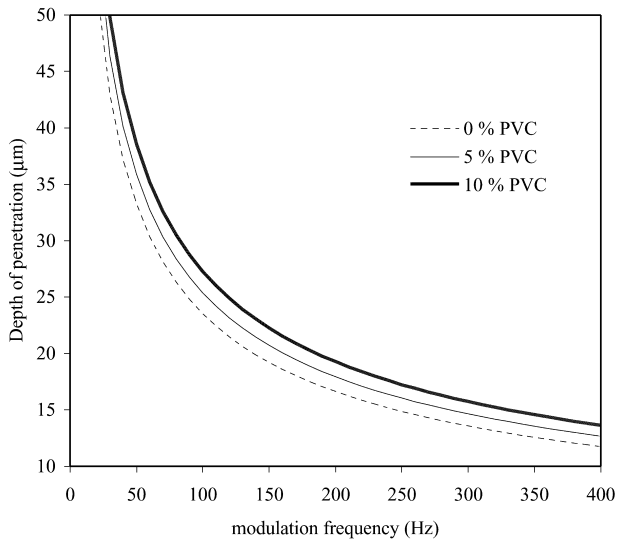

Fig. 7. Depth of penetration plotted as a function of modulation frequency for 0, 5, and 10% PVC.

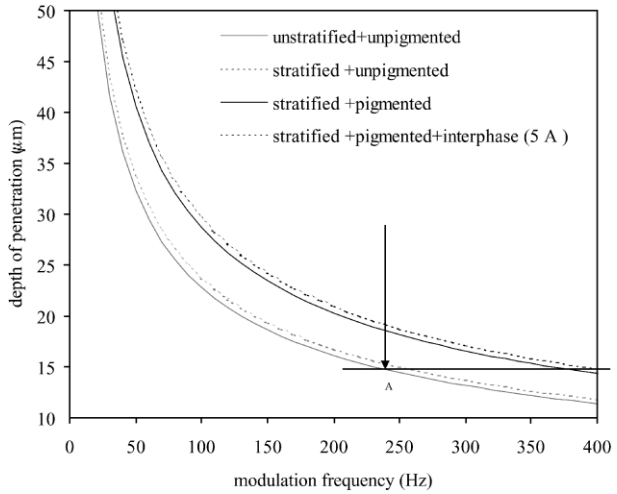

Fig. 8. Depth of penetration plotted as a function of modulation frequency for stratified, non-stratified, pigmented, and non-pigmented PUR films. Point A represents the modulation frequency for non-pigmented PUR films that corresponds to the same depths of penetration achieved for pigmented PUR.

Acknowledgements

The authors are thankful to the National Science Foundation I/U CRC in Coatings for support of these studies.

Appendix A

Algorithms A and B utilized in generating a flowchart illustrated in Fig. 2.

References

[1] Bell AG. Am J Sci 1880;20:305.
[2] Rosencwaig A, Gersho A. J Appl Phys 1976;47:64.
[3] Rosencwaig A. J Appl Phys 1978;64:2905.
[4] Urban MW. Vibrational spectroscopy of molecules and macromolecules on surfaces. NY: Wiley; 1993.
[5] Urban MW. Encyclopedia of vibrational spectroscopy. United Kingdom: Wiley; 2001.
[6] Urban MW, Koenig JL. Appl Spectrosc 1986;40:994.
[7] Carter III RO, Paputa Peck MC. Appl Spectrosc 1989;43:468.
[8] Yang CQ, Ellis TJ, Breese RR, Fately WG. Polym Mater Sci Engng 1985;53:169.
[9] Tiefenthaler AM, Urban MW. Composites 1989;20:145.
[10] Zerlia T. Appl Spectrosc 1986;40:214.
[11] Rosencwaig A. In: Robert E, editor. Photoacoustics and photoacoustic spectroscopy. Malabar, FL: Krieger Publishing; 1980.
[12] Dittmar RM, Chao JL, Palmer R, Springer Series in Optical Sciences: Photoacoustic and Photothermal Phenomena III, vol. 6. Berlin: Springer; 1992. p. 492.
[13] Zhao Y, Urban MW. In: Urban MW, Provder T, editors. Film formation. ACS Symposium Series, #790, Washington, DC: American Chemical Society; 2001.
[14] Zhao Y, Urban MW. Macromolecules 2000;33:8426.
[15] Urban MW, Allison CL, Johnson GL, DiStefano F. Appl Spectrosc 1999;53:1520.
[16] Pennington BD, Urban MW. Polymer 1999;40:1321.
[17] Stegge JM, Urban MW. Polymer 2001;42:5479.
[18] Han Q, Urban MW. J Appl Polym Sci 2001;81:2045.
[19] Katti KS, Urban MW. J Coat Technol 2000;72:35.
[20] Pennington BP, Grunlan JC, Urban MW. J Coat Technol 1999;71:135.
[21] Bhatt H, Donaldson KY, Hasselman DPH, Bhatt RT. J Am Ceram Soc 1990;73:312.
[22] Bhatt H, Donaldson KY, Hasselman DPH, Bhatt RT. J Mater Sci 1992;27:6653.
[23] Powell Jr BR, Youngblood GE, Hasselman DPH, Bentsen LD. J Am Ceram Soc 1980;63:581.
[24] Hasselman DPH, Donalson KY, Geiger AL. J Am Ceram Soc 1992; 75:3137.
[25] Lu S-Y, Song J-L. J Appl Phys 1996;79:609.
[26] Bruggeman DAG. Ann Phys 1935;24:636.
[27] Bergman DJ, Stroud D. Solid State Phys 1992;46:147.
[28] Lu S-Y, Lin H-C. J Appl Phys 1996;79:6761.
[29] Agari Y, Tanaka M, Nagai S. J Appl Polym Sci 1987;34:1429.
[30] Agari Y, Ueda A, Nagai S. J Appl Polym Sci 1991;42:1665.
[31] Agari Y, Uno T. J Appl Polym Sci 1985;30:2225.
[32] Raman K, Vaidyanathan A. J Compos Mater 1995;29:1725.
[33] Katti K, Urban MW. J Coat Technol 2000;72:35.
[34] Touloukian YS, editor. Thermophysical properties of high temperature solid materials. Inter-metallics, cements, polymers, and composite systems, vol. 6.; Macmillan, New York, 1966.
[35] Handbook of chemistry and physics. 54th ed, Boca Raton: The CRC Press; 1973.